Int. J. Multiphase Flow Vol. 13, No. 3, pp. 327–343, 1987
Printed in Great Britain.

0301-9322/87 $3.00 + 0.00

3-D TURBULENCE STRUCTURE AND PHASE DISTRIBUTION MEASUREMENTS IN BUBBLY TWO-PHASE FLOWS

S. K. WANG, S. J. LEE, O. C. JONES JR and R. T. LAHEY JR
Department of Nuclear Engineering & Engineering Physics, Rensselaer Polytechnic Institute, Troy, NY 12180-3590, U.S.A.

(*Received* 1 *January* 1986; *in revised form* 1 *November* 1986)

Abstract—Turbulent bubbly air/water two-phase up and down flows in a circular test section were investigated. Important flow quantities such as local void fraction, liquid velocity and the Reynolds stresses were measured using both single-sensor and three-sensor hot-film anemometer probes. For up flows, it was found that the bubbles tended to migrate toward the wall and thus the void fraction profile showed a distinct peak near the wall. In contrast, for down flows, it was found that the bubbles tended to migrate toward the center of the pipe causing void "coring". It was also found that the observed wall peaking and coring phenomena, and thus the radial void distribution in up and down flows, could be predicted by considering the turbulence structure of the continuous phase and lateral lift force acting on the dispersed phase (i.e. the bubbles).

All Reynolds stress components were measured using a special 3-D conical probe. In two-phase flows, the normal Reynolds stress components (i.e. u^2, v^2 and w^2) showed nearly flat profiles in the core region ($r/R < 0.8$) and, except near the wall, the turbulence structure was more anisotropic compared to single-phase flows. Normally, the presence of the bubbles increased the level of turbulence in the flow. However, because the bubbles in turbulent two-phase flow enhance dissipation as well as promoting the production of turbulence kinetic energy, it was found that for higher flow rates the presence of bubbles suppressed the level of turbulence.

1. INTRODUCTION

One of the most important and yet least understood aspects of two-phase flow are the lateral phase distribution mechanisms which occur. This multidimensional effect is often quite pronounced and must be considered in the accurate analysis of heat and momentum transfer for chemical and power industry applications. Much of the analysis which has been published to date has been concerned with 1-D rather than multidimensional effects. However, the lack of information on transverse phase distribution can result in significant restrictions in many practical applications. For example, the measured flow and enthalpy in the various subchannels of a nuclear fuel rod bundle cannot be predicted using standard subchannel computer codes such as COBRA because the turbulence models in such codes are insufficient to predict the observed lateral void distribution. Therefore, before one can accurately predict such important thermal-hydraulic phenomena as the local critical heat flux (CHF), an accurate flow and void distribution must be predicted.

The purpose of the study presented herein was twofold. The first purpose was to develop reliable methods to measure such two-phase flow parameters as local void fraction, liquid phase velocity and the turbulent stresses. The second purpose was to compare the measured void distribution with the predicted distribution based on a mechanistic model. A unique relationship was deduced between the lateral phase distribution and the structure of turbulence in the continuous phase which confirmed the importance of turbulence modeling in two-phase flows.

Despite numerous experimental and analytical studies of two-phase flow during the past 20 years, no one was able to satisfactorily predict lateral phase distribution. This was due to inadequate two-phase flow constitutive models and insufficient basic two-phase flow data. Several of the most significant previous studies are summarized next.

The lateral void distribution for a bubbly flow was apparently first analyzed by Bankoff (1960). He assumed a power law distribution for both the velocity and the void fraction:

$$\frac{U}{U_{\ell}} = \left(1 - \frac{r}{R}\right)^{\frac{1}{m}} \qquad [1]$$

$$\frac{\alpha}{\alpha_{\ell}} = \left(1 - \frac{r}{R}\right)^{\frac{1}{n}}, \qquad [2]$$

where U is the local mean velocity, α is the local void fraction and the subscript $\mathfrak{L}$ denotes the centerline of the pipe. Thus, the void concentration was assumed to be a maximum at the center of the pipe, decrease monotonically in a radial direction and vanish at the pipe wall.

Levy (1963) extended single-phase turbulent mixing-length methods to two-phase flows and predicted two-phase density and velocity distributions which also peaked at the centerline of the pipe.

Beattie (1972) assumed a linear relationship between the velocity of the continuous phase (liquid) and the void fraction:

$$\alpha = \mathrm{a}\, U_{\mathrm{L}} + \mathrm{b}, \qquad [3]$$

where a and b are constants. He then applied a mixing-length model to [3] to derive a power law void fraction profile which again peaked at the center of the pipe.

Delhaye (1969) derived a radial void fraction profile by solving the two-fluid momentum equations. In his derivation, several key assumptions were made. He used the relative velocity relationship proposed by Zuber *et al.* (1967):

$$(U_{\mathrm{B}} - U_{\mathrm{L}}) = \frac{U_{\infty}}{(1-\alpha)}, \qquad [4]$$

where U_{B} is the bubble velocity and U_{∞} is the bubble's terminal rise velocity. Moreover, the interfacial drag force (F_{D}) was given by

$$\frac{F_{\mathrm{D}}}{\rho_{\mathrm{L}}(U_{\mathrm{B}} - U_{\mathrm{L}})^2 d_{\mathrm{B}}^2} = \mathrm{K}\frac{\nu_{\mathrm{L}}}{\epsilon}\frac{d_{\mathrm{B}}}{(U_{\mathrm{B}} - U_{\mathrm{L}})}\frac{\mathrm{d}}{\mathrm{d}r}(U_{\mathrm{B}} - U_{\mathrm{L}}), \qquad [5]$$

where K is a positive constant and ϵ is the so-called turbulent viscosity,

$$\epsilon \triangleq -\bar{k}^2(R-r)^2\frac{\mathrm{d}}{\mathrm{d}r}(U_{\mathrm{B}} - U_{\mathrm{L}}). \qquad [6]$$

Delhaye finally deduced a power law void fraction profile having a maximum at the pipe centerline.

One of the reasons that Delhaye's model was unable to predict the observed wall peaking of voids is that the turbulent fluctuations of the continuous phase were neglected. As a result, the radial pressure distribution was uniform. Actually, the radial pressure distribution in fully-developed bubbly two-phase flow is not uniform, rather, as given in the Appendix, it is given by

$$p(r) = p(R) - (1-\alpha)\rho_{\mathrm{L}}\overline{v^2} - \int_R^r \frac{(1-\alpha)\rho_{\mathrm{L}}(\overline{v^2} - \overline{w^2})}{r'}\mathrm{d}r', \qquad [7]$$

where v^2 and w^2 are the turbulent fluctuations in the radial and azimuthal directions, respectively. It can be seen that the local static pressure is lowest in the region near the wall where turbulence production is the largest. As will be discussed subsequently, this nonuniform pressure field strongly influences the lateral phase distribution.

Kobayasi *et al.* (1970) proposed an empirical formula to predict the void fraction distribution of bubbly and slug flows. Although this empirical equation successfully predicts the observed void "peaking" near the wall for two-phase up flows, it has no physical basis.

Inoue *et al.* (1976) suggested that the turbulence exchange of momentum between the liquid and vapor phases can be characterized by a mixing length in the liquid phase. Based on the measured shear stress and void fraction distributions, the authors calculated a two-phase mixing length and showed that it is larger than in single-phase flows. They concluded that "wall-peaking" was in some way a result of the two-phase mixing length which also showed a peak near the wall. While the relationship proposed between the structure of turbulence and the lateral void distribution appears to be reasonable, lateral life was not considered, nor was a functional form of the two-phase mixing length given by the authors. Unfortunately, this seriously limits the usefulness of their results.

Based on above discussion, it can be concluded that most previous analytical investigations either did not predict the observed phenomena, shed any new light on the physical mechanisms controlling lateral phase distribution or were not complete enough to allow for accurate predictions.

Perhaps the most important quantity in modeling the lateral phase distribution is the turbulence structure. The turbulence structure was successfully incorporated into the modeling of phase distribution by Drew *et al.* (1978), Drew & Lahey (1979, 1981, 1982) and Lahey & Drew (1979). Making reasonable assumptions about fully-developed two-phase flow, the authors were able to integrate the phasic momentum equations of a two-fluid model analytically. The resultant radial void fraction distribution was given by

$$\frac{\alpha^q}{(1-\alpha)} = \hat{C}_2\left[\frac{K_{z_L}(r)F_r(r)}{F_z(r)}\right]^{1-q} e^{-(1-q)\int_0^r \frac{[F_\theta(r')-F_r(r')]}{rF_r(r')}dr'}, \quad [8]$$

where $K_{ik} \triangleq \frac{1}{2}\rho_k \overline{u_{ik}^2}$ is the turbulent kinetic energy in direction i for phase k,

$$F_i \triangleq \frac{\overline{u_i^2}}{\sum_j \overline{u_j^2}}$$

is the (anisotropic) ratio of the directional liquid-phase turbulent kinetic energies to the total liquid-phase kinetic energy, $q = K_{z_G}/K_{z_L}$ is the constant of proportionality between the turbulent kinetic energies of each phase and $\hat{C}_2$ is the integration constant. Clearly, the void distribution depends on the structure of the liquid-phase turbulence. Although all interfacial forces in the radial momentum equations were neglected by Drew & Lahey (1982), their model qualitatively predicted the void peaking phenomenon for bubbly two-phase up flow if the appropriate turbulence structure of the continuous phase was prescribed. Subsequently, the authors extended this model to down flows (Drew & Lahey 1982). By using mixing-length theory to model the turbulence stresses in the continuous phase, they showed that for down flows the lateral void distribution peaked at the center of the conduit instead of near the wall. This "coring" of the vapor phase in down flow agreed qualitatively with the measurements of Oshinowo & Charles (1974).

As can be seen in [7], turbulence induces a lateral pressure gradient which, because of differences in the axial inertia of the vapor and liquid phases, causes the vapor phase to preferentially collect in low-pressure zones, thus leading to a nonuniform lateral void distribution. In addition, interfacial forces such as the drag force, lift force, virtual mass force, Basset force and Faxen force may also play an important role. In steady fully-developed two-phase pipe flow with no swirl, lateral lift forces exist in the radial direction. In dispersed bubbly two-phase flow, the lift force is due to an unbalanced pressure distribution around the interface resulting from interaction with the liquid-phase shear gradient. Therefore, in order to accurately predict the lateral void distribution, both the turbulence structure and the lateral lift force should be incorporated into the analysis. The derivation of a mechanistic model for void distribution which includes both effects will be presented in section 7 of this paper.

2. DISCUSSION

There have been thousands of papers published on either void fraction or single-phase turbulence measurements. Unfortunately, there have only been a few publications concerned with the turbulence structure of two-phase flows.

Serizawa (1974; Serizawa *et al.* 1974a–c) studied turbulent fully-developed two-phase bubbly up flows in a circular conduit. He used electrical resistivity probes to measure the local void fraction, the bubbly impaction rate, the bubble velocity and its spectrum. Turbulence quantities, such as the liquid-phase mean velocity, and the axial turbulent fluctuations were measured using a hot-film anemometer. He reported that the vapor-phase distribution was nearly uniform in the pipe's core region and was peaked near the wall. Interestingly, the bubble velocity, the water velocity and the local relative velocity showed fairly flat profiles in the radial direction without any maxima near the wall. More recently, Serizawa *et al.* (1983; Serizawa & Michiyoshi 1984) used a dual-sensor hot-film probe (a miniature X-type film probe) to measure the axial and radial turbulent fluctuations and the Reynolds stress. The bubble-induced velocity fluctuations were found to increase with local void fraction. The authors also claimed that the data indicated nearly isotropic behavior for highly turbulent bubbly flows—an observation not supported by the data presented herein.

Lance (1979; Lance *et al.* 1980) reported grid-generated turbulent two-phase flow measurements in a large square channel. The void fraction, the liquid velocity and the axial velocity fluctuations were measured using a conical hot-film probe. The author concluded that in the absence of any mean velocity gradient, the axial turbulent fluctuation intensity increased as a function of void fraction. However, since the maximum void fraction in his investigation was <3%, these conclusions are not general.

Marié & Lance (1983) measured the turbulent fluctuations in two-phase flows using a laser–Doppler anemometer (LDA) system. Their study was restricted to low void fractions, and also showed that the turbulent fluctuations increased with void fraction.

Sullivan *et al.* (1978) and Theofanous & Sullivan (1982) measured the axial and radial turbulent fluctuations in a circular channel by using both a hot-film anemometer and an LDA system in dispersed bubbly flows. The authors predicted the axial fluctuation at the pipe's centerline by assuming that the turbulence level in the liquid phase is the sum of wall-induced and bubble-induced turbulence. Although the predictions agreed well with their data, the model was never tested for highly turbulent flows where other investigators (e.g. Tsuji *et al.* 1984) found that the dissipative effects of the bubbles dominate.

From the above discussion, it is clear that the previous experiments on turbulent two-phase flows were incomplete. On the other hand, we need information on two-phase flow turbulence if many important problems in two-phase flow are to be solved, such as phase distribution. It was the purpose of the present research to develop a consistent and reliable methodology with which to measure the 3-D turbulence quantities and the void fraction in two-phase flows, to take a complete set of such data, and to compare these data to a mechanistic model for the lateral phase distribution.

3. EXPERIMENTAL METHODS

The air/water loop shown schematically in figure 1 had a 57.15 mm i.d. test section which could be turned upside down to allow for measurements of both up and down flows. A single sensor cylindrical hot-film probe, TSI-1218-20W, was used to measure the mean and fluctuations in the axial liquid velocity, and the local void fraction. To measure the Reynolds stress components (i.e. $\overline{u^2}$, $\overline{v^2}$, $\overline{w^2}$, $\overline{uv}$, $\overline{vw}$, $\overline{uw}$) in the liquid phase, a special 3-D conical probe, shown in figures 2 and 3, was used. Compared to commercially-available 3-D probes, this probe was more rugged, less susceptible to contamination and much smaller. The frequency response of the 3-D conical probe was evaluated and it was found that all three sensors on the probe respond to the velocity fluctuations with frequencies up to 10 kHz without significant attenuation (Wang 1985).

In order to relate the probe signals to the Reynolds stresses, the velocity vector can be decomposed into the components perpendicular and tangential to each sensor by appropriate coordinate transformations. Then the effective velocities measured by each sensor can be determined using calibration data for the cooling factors. The six† fundamental components of the Reynolds stress tensor were thus determined by

$$\mathbf{u} = \mathbf{A}^{-1}\,\mathbf{e}, \qquad [9]$$

where $\mathbf{e} = (\overline{e_1^2}, \overline{e_2^2}, \overline{e_3^2}, \overline{e_1 e_2}, \overline{e_1 e_3}, \overline{e_2 e_3})^{\mathrm{T}}$ and e_i are the effective signals measured on sensor i, $\mathbf{u} = (\overline{u^2}, \overline{v^2}, \overline{w^2}, \overline{uv}, \overline{uw}, \overline{vw})^{\mathrm{T}}$ designates the Reynolds stresses (divided by $-\rho_{\mathrm{L}}$) and $\mathbf{A}$ is a 6×6 matrix used for the coordinate transformations (Wang 1985). To verify the above method, a 45° cylindrical probe was also used to measure $\overline{u^2}$, $\overline{v^2}$ and $\overline{uv}$ in the core region by rotating the probe into three different orientations. The analytical basis for the measuring technique using a 45° probe has been given by Wang (1985).

The anemometer signal was sampled at 10 kHz using an A/D converter and the results were fed into a minicomputer for processing. To discriminate the vapor phase (i.e. air) from the liquid phase, a method combining level and slope thresholding was used (Wang 1985). Figure 4 is a schematic of a typical signal and the corresponding position of the bubble with respect to the probe. Note that the vapor phase spans times from time t_{A} to t_{C}, while sharp changes in the signal occur only

†Note that symmetry arguments yield all nine components of the Reynolds stress tensor from these six components.

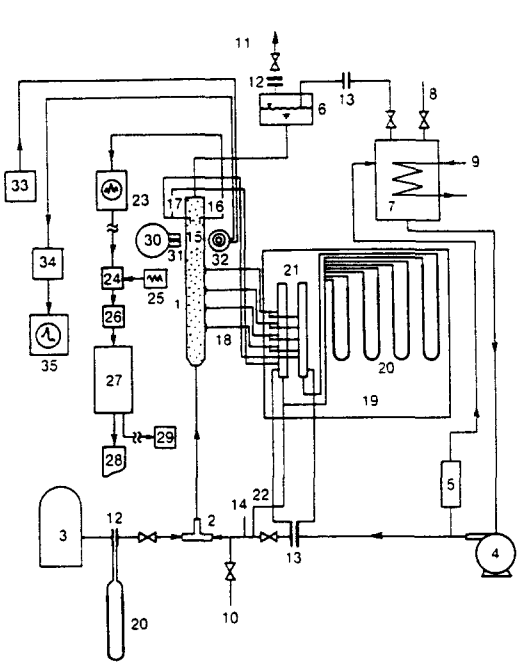

Figure 1. Schematic of the experimental facility.

at t_B and t_C. Thus the measured local void fraction normally underestimates the actual value. The error in the local void fraction measurements was determined using a single-beam γ-ray densitometer as a standard and corrections were made.

4. VOID FRACTION DATA

A void fraction correction method based on measured local parameters and the γ-ray densitometer results was developed by Wang *et al.* (1984). This correction method was based on the parameter, We d_B/d_p, where We is the bubble Weber number and d_B and d_p are the diameters of the bubble and probe, respectively. For up flows, this method gave results consistent with the γ-ray measurements. Unfortunately, the method was never calibrated for down flows, thus an alternate method for void fraction correction was needed for down flows. Fortunately, one can also infer void distribution from the $\overline{uv}$ measurements. As shown by Wallis (1969), for fully-developed two-phase flow in a vertical pipe the shear stress distribution can be found by balancing the forces acting on a cylinder of radius r. The result is

$$\tau_L(r) = \frac{r}{2(1-\alpha)}\left(-\frac{dp}{dz} - \rho_L g\right) - \frac{g(\rho_L - \rho_G)}{r(1-\alpha)}\int_0^r (1-\alpha)r'dr', \qquad [10]$$

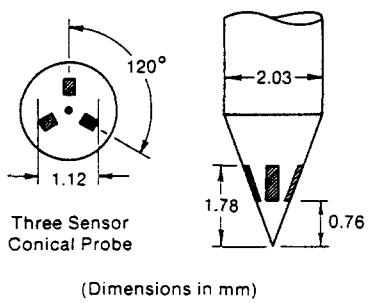

Figure 2. The 3-D conical probe.

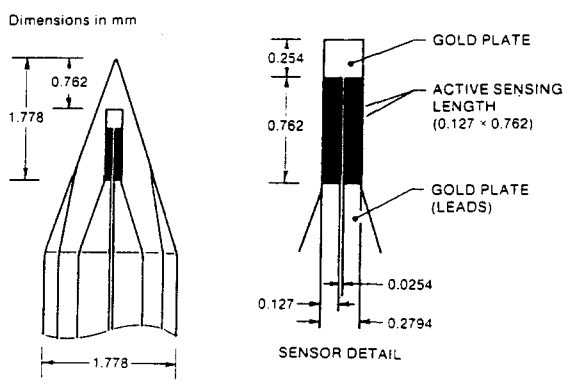

Figure 3. Dimensions of the 3-D conical probe.

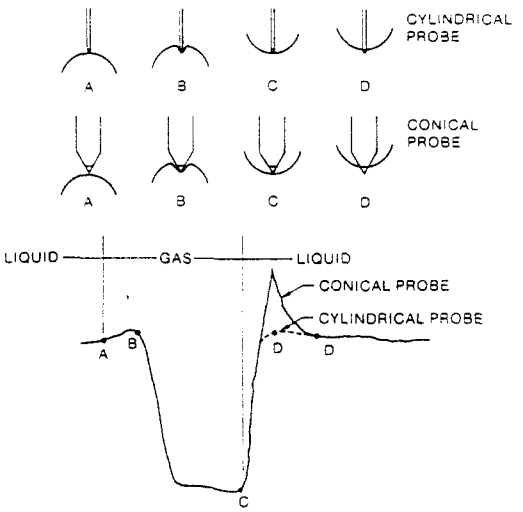

Figure 4. Anemometer signal response of bubble penetration.

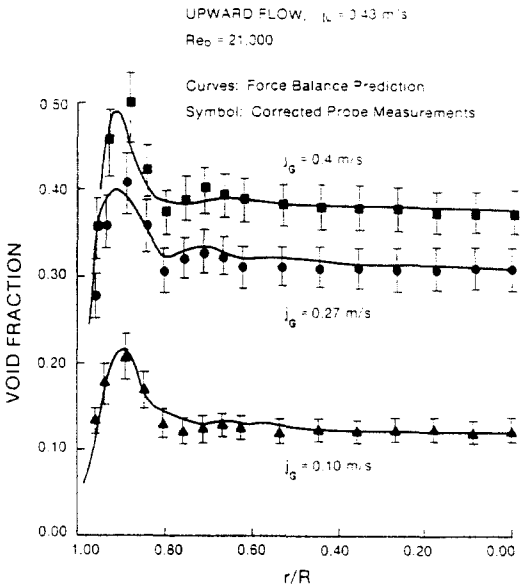

Figure 5. Void fraction profiles.

where $\tau_L = -\rho_L \overline{uv}$ is the turbulent shear stress and the axial pressure gradient, dp/dz, is known since it was measured from the pressure taps along the test section.

Typical void distributions were predicted using the measured values of $\tau_L(r)$ and dp/dz, and the force balance, [10]. These distributions are shown with corrected void data in figures 5–10, where the error bars were worked out using standard propagation-of-error techniques. For up flows, they agree very well, thus supporting the accuracy of the Reynolds stress measurements using the 3-D conical probe. However, because the 3-D conical probe had a spatial resolution of ± 1 mm, it could not resolve the rapid spatial variation of $\overline{uv}$ near the wall, thus some discrepancies exist near the wall, especially for high flows.

Because of buoyancy, in down flows one expects the probe to deform and deflect bubbles even more severely than for up flows. As shown in figures 8–10, the down flow void data, corrected based on the up flow correlation, agrees well in the core region with the void profile deduced from the force balance, but differs near the wall. Because of the good agreement for up flows, the predicted void distribution using the force balance is considered to be more accurate for down flows. A check on liquid mass continuity supports this conclusion (Wang 1985).

The void fraction profiles for down flows are quite different from those for up flows. For down flows, the void fraction stays nearly constant in the core region and then drops abruptly to zero

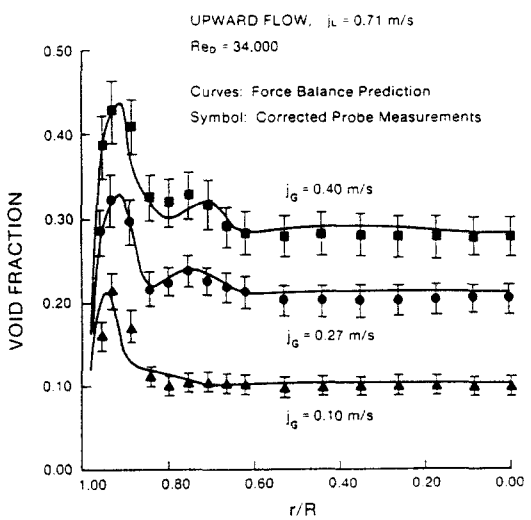

Figure 6. Void fraction profiles.

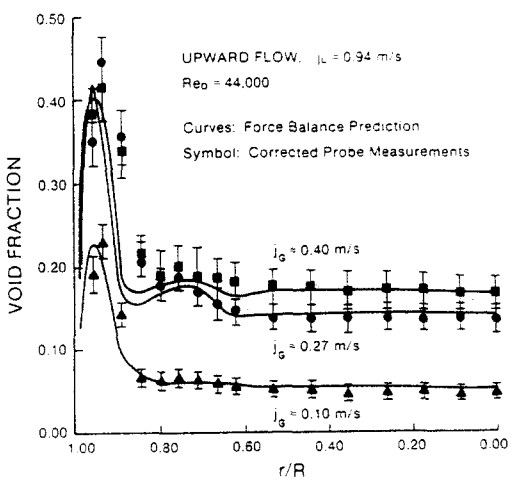

Figure 7. Void fraction profiles.

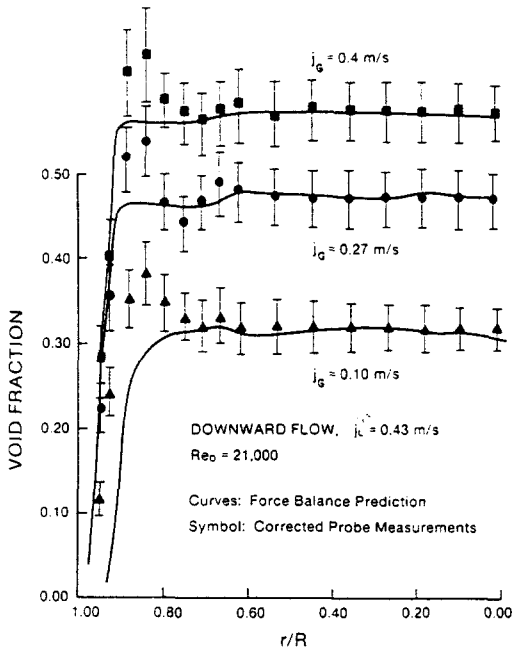

Figure 8. Void fraction profiles.

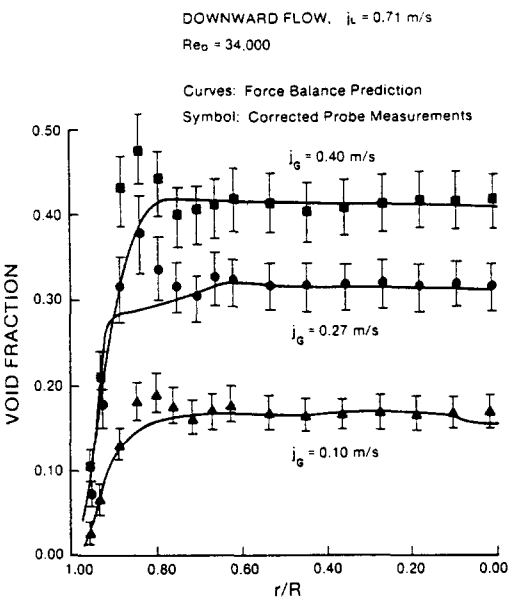

Figure 9. Void fraction profiles.

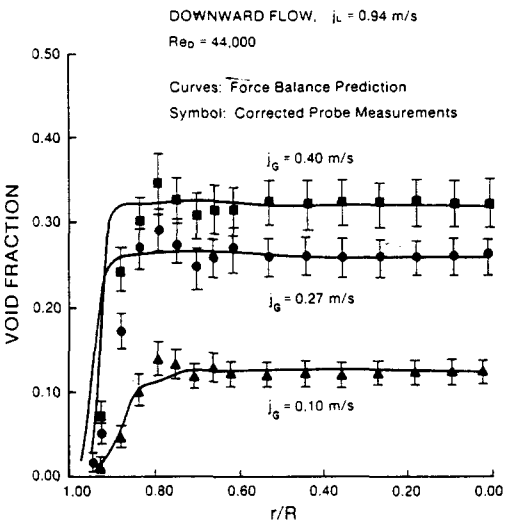

Figure 10. Void fraction profiles.

as the wall is approached. As discussed previously, void "coring" has been reported previously by Oshinowa & Charles (1974) and was predicted qualitatively by Lahey & Drew (1982). In this study it was found that for up flows "wall-peaking" became more pronounced for higher liquid flows, while liquid flow rate appeared to have little effect on the void fraction profiles for down flows.

5. AXIAL LIQUID VELOCITY

Figures 11–14 show some results of the 1-D cylindrical probe measurements. As expected, for the same flow rate single-phase down flows have the same mean liquid velocity and axial fluctuation profiles as those in up flows. In two-phase flows, the presence of voids tends to flatten the liquid velocity profile for both up and down flows. Moreover, for high flows in the upward direction and for the most down flows, the location of the maximum liquid velocity occurred off the pipe's centerline. For up flows, the higher vapor concentration near the wall apparently causes the liquid to move faster due to bubble-induced drag. Similar trends have been reported by Malnes (1966)

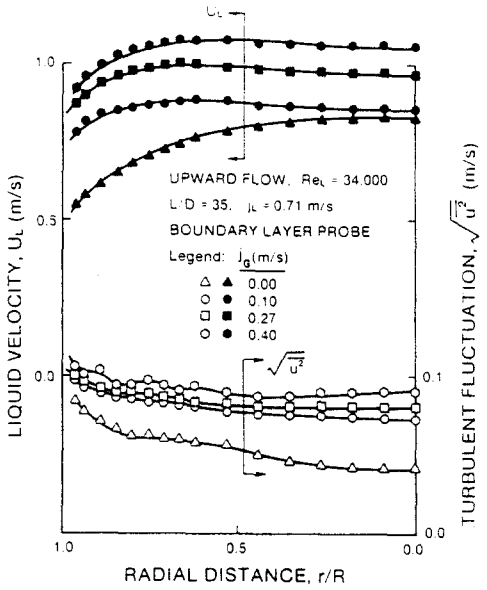

Figure 11. Liquid velocity and turbulent fluctuations.

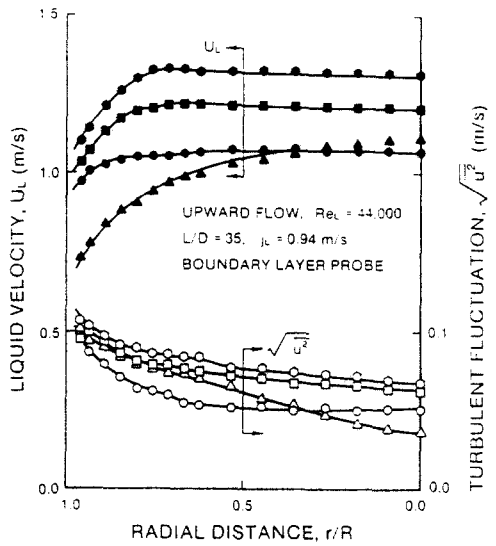

Figure 12. Liquid velocity and turbulent fluctuations. (See figure 11 for symbols.)

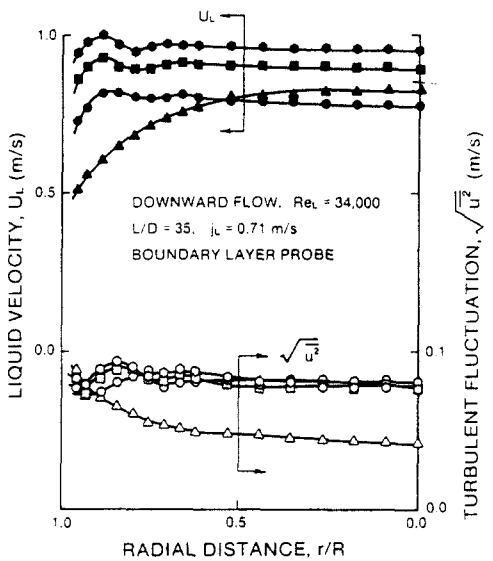

Figure 13. Liquid velocity and turbulent fluctuations. (See figure 11 for symbols.)

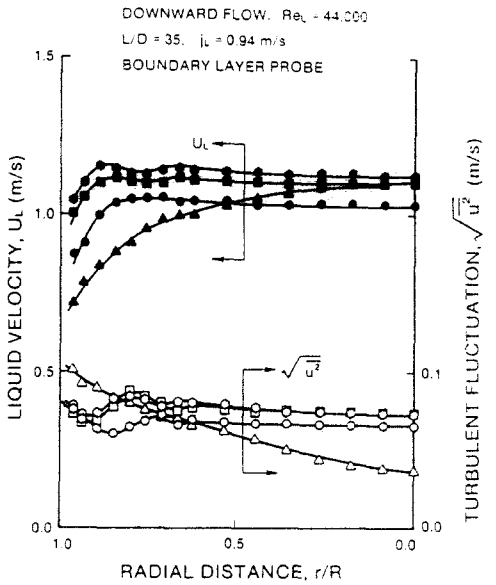

Figure 14. Liquid velocity and turbulent fluctuations. (See figure 11 for symbols.)

and Theofanous & Sullivan (1982), and were termed the "chimney effect." Note that the maximum liquid velocity and the void peak did not occur at the same location, probably because of the counteracting effect of high shear stress near the wall. On the other hand, bubble "coring" in down flows retards the flow in the core due to buoyancy, and the resultant diversion of liquid into the low void region near the wall apparently causes the maximum liquid velocity to again occur near the wall.

6. TURBULENCE STRUCTURE

Typical Reynolds stresses measured with the 3-D conical probe are shown in figures 15–18. The cross terms, $\overline{uw}$ and $\overline{vw}$, are not shown since they are zero in fully-developed pipe flows (Laufer 1953). These quantities were actually measured and found to be essentially zero within the

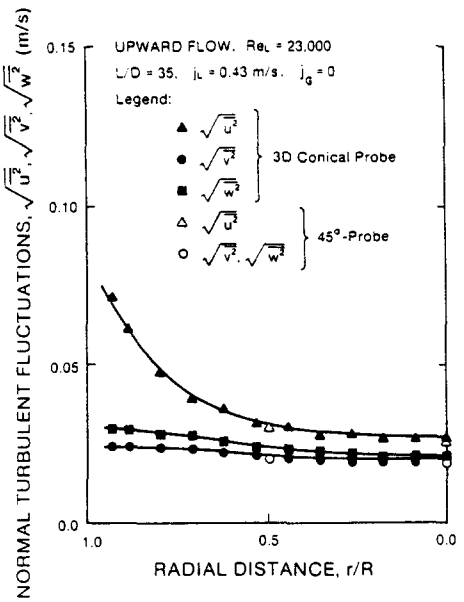

Figure 15. Normal turbulent fluctuations.

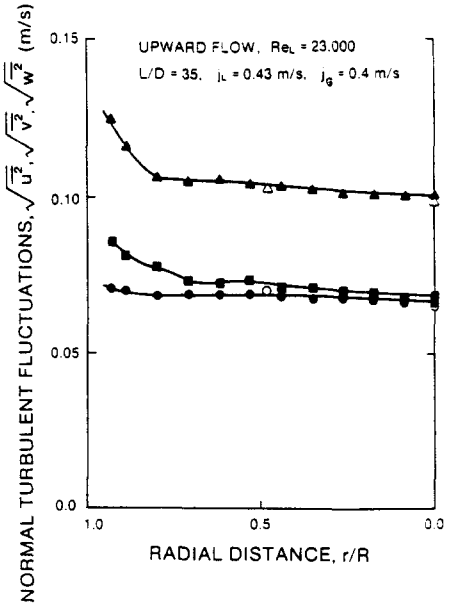

Figure 16. Normal turbulent fluctuations. (See figure 15 for symbols.)

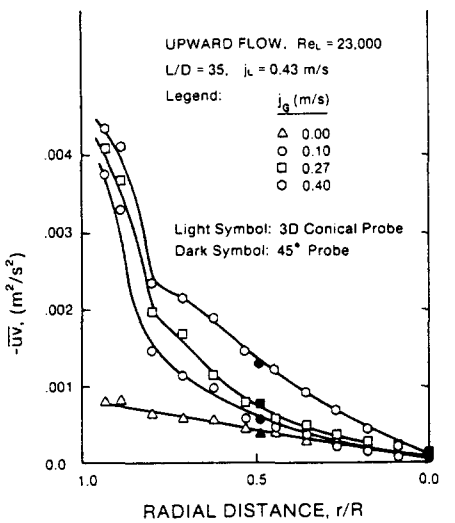

Figure 17. $-\overline{uv}$ Measurements.

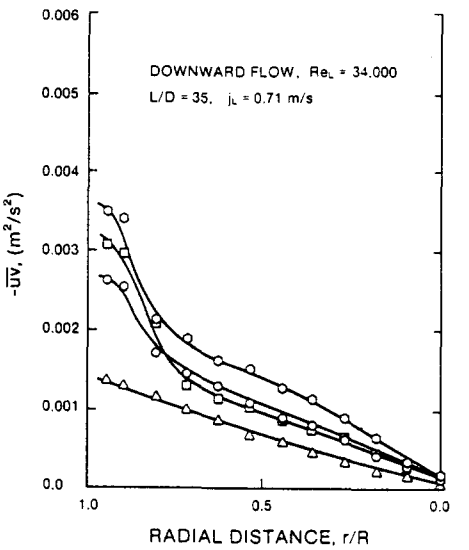

Figure 18. $-\overline{uv}$ Measurements. (See figure 17 for symbols.)

experimental error. Moreover, when the simultaneous equations were solved with $\overline{uw}$ and $\overline{vw}$ set to zero, the other Reynolds stress components, $\overline{u^2}$, $\overline{v^2}$, $\overline{w^2}$ and $\overline{uv}$, were not strongly affected. To verify the consistency and the accuracy of the 3-D conical probe measurements, a 45° cylindrical probe was used for various up flows to measure $\overline{u^2}$, $\overline{v^2}$ and $\overline{uv}$ in the core region. As shown in figures 15–17, these independent results agreed quite well.

It is also significant to note in figures 17 and 18 that the Reynolds stress term $(-\overline{uv})$ was never negative. In particular, it was always positive in the region of the flow field in which the local maximum in the mean liquid velocity occurred. Since the velocity gradient changes sign, it appears that Boussinesq-type models of the form

$$\tau_{Re} = \rho_L (1-\alpha)(\nu_L + \epsilon_L)\frac{dU_L}{dr} \qquad [11]$$

are inadequate to describe the observed data trends.

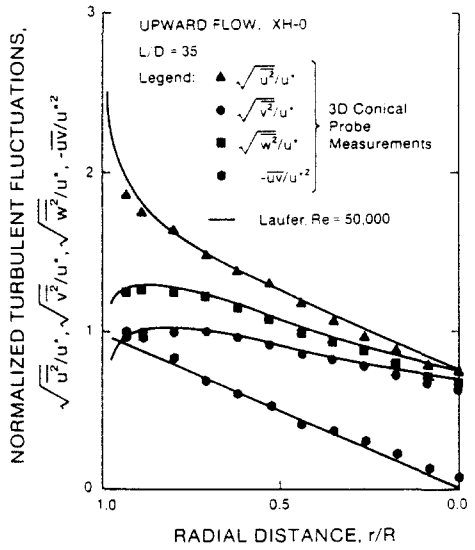

Figure 19. Comparison of single-phase turbulent fluctuations.

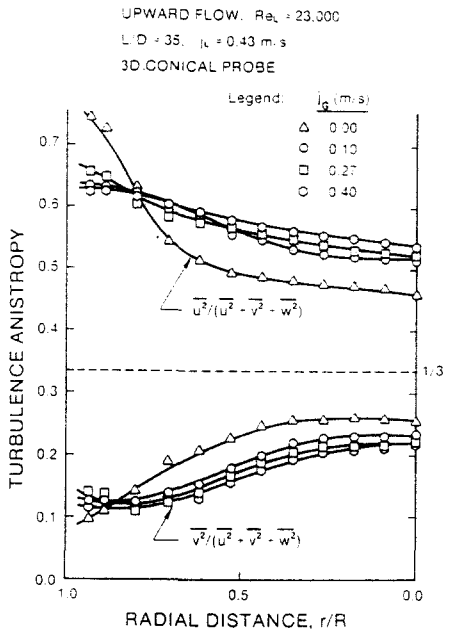

Figure 20. Radial variation of turbulence anistropy.

A complete set of single-phase turbulence measurements were made by Laufer (1952, 1953). He used a hot-wire anemometer to measure turbulence parameters such as the velocity profile, turbulent fluctuations in the three orthogonal directions, the Reynolds stresses and some other statistical quantities of interest. His results have been widely employed to check the validity of other single-phase turbulence measurements. As can be seen in figure 19, our single-phase turbulence data agreed quite well with Laufer's data, thus further verifying our experimental techniques.

Normally, the turbulence level increased rapidly to a certain value when a small amount of vapor was introduced in to a single-phase flow. Thereafter, additional amounts of vapor had less effect. However, for more highly turbulent flows (i.e. for higher liquid flow rates), the presence of vapor decreased the turbulence level, as can be seen in figures 12 and 14. This observation clearly shows that the widely accepted superposition hypothesis, which implies that the turbulence level in two-phase flow is the sum of the turbulence due to wall-shear-induced and bubble-induced turbulence is invalid. Indeed, according to this hypothesis the turbulence level should increase monotonically with vapor content; obviously this is not always the case.

A reduction in the two-phase turbulent fluctuations has also been observed by Serizawa (1974) and Tsuji *et al.* (1984). Serizawa ascribed this phenomenon to competition among the following effects:

(1) A decrease in the effective volume of the liquid phase for energy dissipation due to the volume occupied by the bubbles—the effect being to increase the fluctuations.
(2) Work done in providing buoyancy to the bubbles—the effect serves to reduce the fluctuations.
(3) Energy dissipation associated with the lateral relative motion or rotation of the bubbles—the fluctuations may be decreased in order to supply this energy dissipation.
(4) The energy-absorbing character of bubbles—the bubbles may act as an energy sink to reduce the fluctuations.

It is believed that the fourth effect accounts for most of the reduction in the turbulence, however a detailed modeling of energy production and dissipation mechanisms is needed to accurately analyze turbulent two-phase flow.

The local isotropy of the three normal fluctuations is also affected by the presence of the vapor phase. By introducing the vapor phase, the turbulence structure first becomes more anisotropic

everywhere except in the region near the wall. Thereafter the anisotropy is hardly affected by introducing more vapor. The typical radial variation of the anisotropy of the turbulence structure for single- and two-phase flows is shown in figure 20.

7. PREDICTION OF RADIAL VOID DISTRIBUTION

Let us now derive an expression for the radial void distribution in fully-developed turbulent pipe flow using the radial momentum conservation equations. Ishii (1975) has formulated a two-fluid model by considering the conservation laws for each phase separately. By making the same assumptions as made previously by Drew *et al.* (1978), the radial momentum equation can be simplified to

$$-\alpha\frac{\partial p}{\partial r}+\frac{1}{r}\frac{\mathrm{d}}{\mathrm{d}r}(\alpha r\tau_{rr_G})-\frac{1}{r}\alpha\tau_{\theta\theta_G}+M_L=0, \qquad [12a]$$

for the vapor phase, and

$$-(1-\alpha)\frac{\partial p}{\partial r}+\frac{1}{r}\frac{\mathrm{d}}{\mathrm{d}r}[r(1-\alpha)\tau_{rr_L}]-\frac{1}{r}(1-\alpha)\tau_{\theta\theta_L}-M_L=0, \qquad [12b]$$

for the liquid phase.

As shown by Drew & Lahey (1979, 1982) and Thomas *et al.* (1983), the interfacial lift force vector, $\mathbf{M}_L$, can be expressed as

$$\mathbf{M}_L=A\rho_L\alpha(\mathbf{U}_L-\mathbf{U}_G)\times\nabla\times\mathbf{U}_L. \qquad [13]$$

For the special case of a spherical bubble immersed in an inviscid liquid (i.e. a liquid having an infinite Reynolds number), the lift parameter (A) can be shown to be 0.5 (Drew & Lahey 1979). Moreover, for fully-developed, axisymmetric pipe flow, the lift force given in [13] reduces to

$$M_L=A\rho_L\alpha(U_L-U_G)\frac{\partial U_L}{\partial r}. \qquad [14]$$

The radial pressure gradient ($\partial p/\partial r$) in the momentum equations can be eliminated by combining [12a] and [12b]. If we then assume $\rho_G/\rho_L\simeq 0$, neglect the shear stress in the vapor phase and recall that

$$\tau_{rr_L}=-\rho_L\overline{v^2} \qquad [15]$$

and

$$\tau_{\theta\theta_L}=\rho_L\overline{w^2}, \qquad [16]$$

we obtain

$$\frac{\mathrm{d}(1-\alpha)}{\mathrm{d}r}+F(r)(1-\alpha)=G(r). \qquad [17]$$

Equation [17] is a Bernoulli-type differential equation which integrates to

$$\alpha(r)=1-\left\{(1-\alpha_\ell)+\int_0^r G(r'')\exp\left[\int_0^{r''}F(r')\mathrm{d}r'\right]\mathrm{d}r''\right\}\exp\left[-\int_0^r F(r')\mathrm{d}r'\right], \qquad [18]$$

where

$$F(r)\triangleq\frac{1}{\overline{v^2}}\frac{\mathrm{d}\overline{v^2}}{\mathrm{d}r}+\frac{1}{r}\left(1-\frac{\overline{w^2}}{\overline{v^2}}\right) \qquad [19]$$

and

$$G(r)\triangleq A\left(\frac{U_G-U_L}{\overline{v^2}}\right)\frac{\mathrm{d}U_L}{\mathrm{d}r}. \qquad [20]$$

If we neglect the lift force term in [18] (i.e. set $A=0$), we obtain [8], which, for $q=0$, is the same result previously derived by Lahey & Drew (1978).

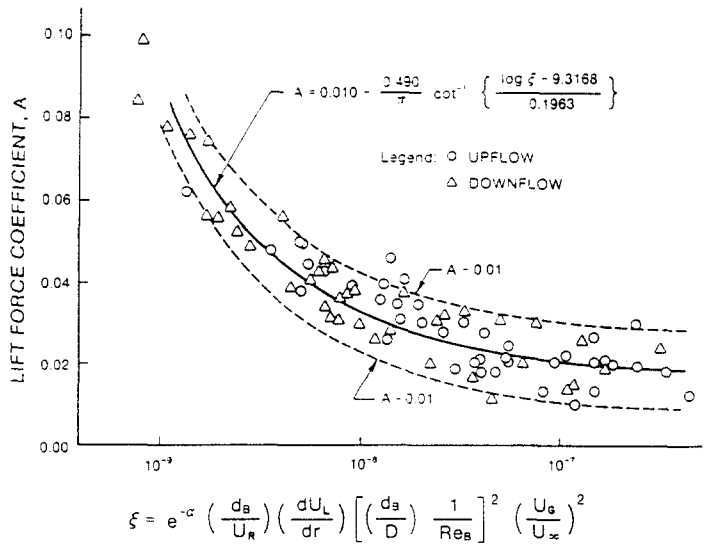

Figure 21. The lift force coefficient.

Since the lift force coefficient, A, was not known for a finite Reynolds number, it was determined by evaluating A from [18], in which representative data was used for $\alpha(r)$, $F(r)$ and $G(r)$. In correlating the lift force coefficient, A, the approach previously proposed by Eichhorn & Small (1964) was employed. They investigated the fluid dynamic forces on spheres suspended in Poiseuille flow. By considering the forces on a sphere, the authors correlated the lift force coefficient and found that it was a function of some local parameters, such as particle Reynolds number, velocity gradient, particle diameter, pipe diameter and the relative velocity. Using the same local parameters and the local void fraction, a dimensionless parameter, ξ, which is a generalization of that proposed by Eichhorn & Small (1964) was deduced. This parameter is given by

$$\xi \triangleq e^{-\alpha} \frac{d_B}{U_R} \frac{dU_L}{dr} \left(\frac{d_B}{D} \frac{1}{Re_B}\right)^2 \left(\frac{U_G}{U_\infty}\right)^2, \quad [21]$$

where $Re_B \triangleq U_R d_B / \nu_L$ is the bubble Reynolds number, $U_R = (U_G - U_L)$ is the relative velocity and U_∞ is the bubble's terminal rise velocity, given by

$$U_\infty = 1.18 \left(\frac{g\sigma}{\rho_L}\right)^{1/4}. \quad [22]$$

As shown in figure 21, the parameter ξ was found to correlate representative data reasonably well. As ξ decreases, the lift force increases to 0.5 as the bubble Reynolds number approaches infinity (i.e. inviscid flow). When ξ is very large, the lift force coefficient approaches 0.01. The lift force coefficient measured by Eichhorn, C_L, can be related to our lift coefficient, A, as follows.

The force, F_L, measured by Eichhorn & Small (1964) is given by

$$F_L = C_L \tfrac{1}{8} \rho_L (U_L - U_s)^2 \pi d_s^2, \quad [23]$$

where d_s is the sphere's diameter and U_s is the sphere's velocity. It can be written as the lift force per unit volume, as expressed in [14], through the relationship

$$M_L = F_L \left[\frac{\alpha}{\frac{1}{6}\pi d_s^3}\right]. \quad [24]$$

Thus,

$$A = \frac{\frac{3}{4}(U_L - U_s)}{d_s \dfrac{dU_L}{dr}} C_L. \quad [25]$$

The lift force coefficients (i.e. the As) of the sphere/liquid system used by Eichhorn were evaluated using [25] and found to be $\leqslant 0.01$, which is close to our data for large ξ and small α,

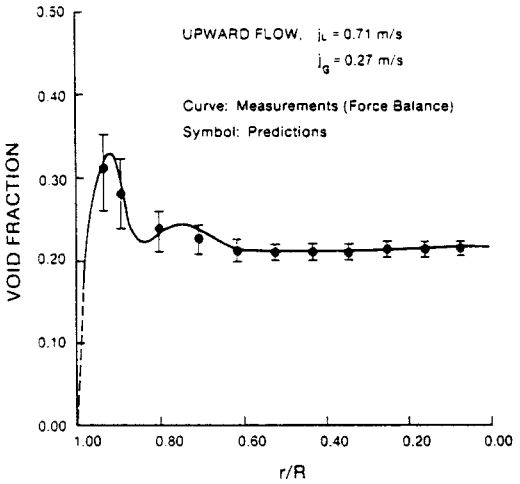

Figure 22. Prediction of the void fraction profile.

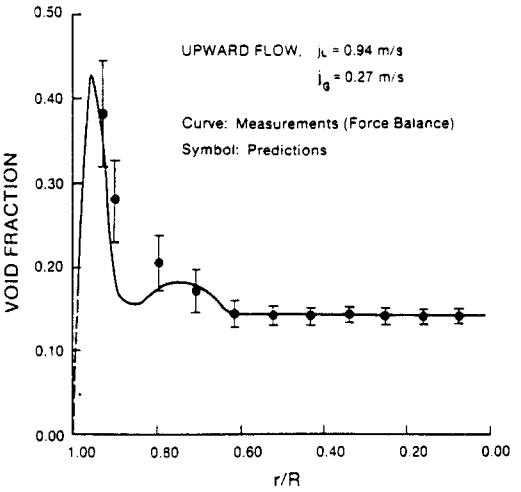

Figure 23. Prediction of the void fraction profile.

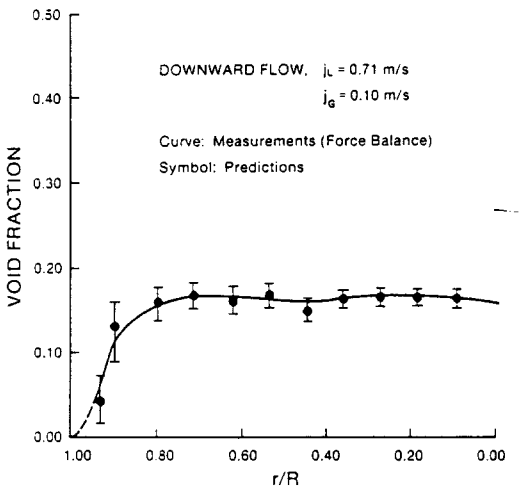

Figure 24. Prediction of the void fraction profile.

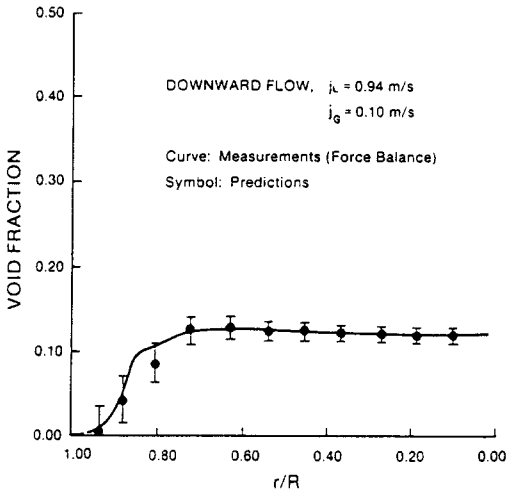

Figure 25. Prediction of the void fraction profile.

For convenience, figure 21 was fitted by a trigonometric function,

$$A = 0.01 + \frac{0.49}{\pi} \cot^{-1}\left(\frac{\log \xi + 9.3168}{0.1963}\right). \qquad [26]$$

Equations [26] and [14] can then be used with [18] to calculate the effect of the lift force on the predicted radial void distributions. Using our data to evaluate the r.h.s. of [18], the local void fraction, $\alpha(r)$, could be predicted. Typical predictions are shown in figures 22–25. Since the lift force coefficients scattered about the correlation curve given in [26] by about ± 0.01, values of $A \pm 0.01$ were used to estimate the sensitivity of the predicted void distribution to uncertainties in the lateral lift force coefficient, A. Normally, the predictions agreed with measurements within the error bands. Note that the greatest discrepancy occurred near the wall because, as can be seen in [14], errors in A are amplified there due to the large velocity gradient in that region. Nevertheless, the wall-peaking and coring of voids in up flows and down flows, respectively, are well-predicted using the model described in this section. Thus, it has been demonstrated that the turbulence-induced lateral pressure field and the lateral lift forces determine how the voids distribute radially. This implies that to accurately predict lateral phase distribution, one must be able to accurately predict the turbulent structure of the continuous phase. While this is currently a state-of-the-art problem it is clear that it is an important area for future research.

8. SUMMARY AND CONCLUSIONS

In order to better understand phase distribution mechanisms, both 1-D and 3-D hot-film anemometer probes were used to measure the void distribution and the turbulence structure of the continuous phase. The void fraction in up and down flows showed two distinct lateral profiles. For up flows the void fraction profile exhibited a sharp peak near the wall. In contrast, for down flows, the voids migrated toward the center of the pipe and formed a pronounced vapor core, while the wall region was relatively free of voids.

In general, the liquid velocity profile was flattened by the presence of the vapor phase (i.e. the bubbles). However, a "chimney effect", in which the maximum liquid velocity occurs away from the pipe's center, was observed. Indeed, for some down flows the maximum velocity occurred very close to the wall. Moreover, all three normal fluctuations were affected by the presence of the vapor phase. Interestingly, these fluctuations do not increase monotonically as the void fraction increases. The presence of bubbles in turbulent flows enhances dissipation of turbulent kinetic energy as well as promoting its production. In some cases, the increase in dissipation rate prevails over the increase in production rate to give net turbulence suppression. The vapor phase also redistributes the radial variation of the turbulent fluctuations. In the core region, the normal turbulent fluctuations and the void fraction frequently showed flat profiles.

A unique relationship between the void fraction distribution and the turbulence structure in the continuous phase was derived. This analytical model indicates the importance of turbulence modeling in two-phase flow analysis. It also showed that the voids distribute as a result of the interfacial lift force and the turbulence-induced lateral pressure distribution. Using representative void fraction and turbulence data, the lift force coefficient was computed for different flow conditions and the results were then correlated. When this correlation was used with the analytical model, both the wall-peaking and coring phenomena seen in all the void fraction data reported herein, for up and down flows, were predicted. The unique relationship between the void fraction distribution and the turbulence structure in the continuous phase clearly indicates the importance of turbulence modeling in two-phase flow analysis.

Acknowledgement—The authors gratefully acknowledge the financial support given to this project by the National Science Foundation (NSF).

NOMENCLATURE

A = Lift force coefficient
$\hat{C}_2$ = Integration constant
C_L = Lift force coefficient
d_B = Bubble diameter
d_p = Probe diameter
F_D = Interfacial drag force
$F_i \triangleq \overline{u_i^2} / \sum_j \overline{u_j^2}$
F_L = Lift force
g = Gravitational constant
j_L = Superficial liquid velocity
j_G = Superficial vapor velocity
K = Turbulent kinetic energy
k = Mixing-length constant
$K_{ik} \triangleq 0.5\, \rho_k\, \overline{u_{ik}^2}$
L/D = Length-to-diameter ratio
M_L = Lift force vector per unit volume
p = Pressure
$q \triangleq K_{zG}/K_{zL}$
r = Radial distance

R = Pipe radius
Re_L = Liquid-phase Reynolds number
U_k = Mean velocity of phase k
$u_L^* \triangleq \sqrt{\tau_w/\rho_L}$, Friction velocity
We = Weber number
$\overline{u^2}$, $\overline{v^2}$, $\overline{w^2}$, $\overline{uv}$, $\overline{uw}$, $\overline{vw}$ = Reynolds stresses ($\div -\rho_L$) in the liquid phase

Greek

α = Local void fraction
α_{ℓ} = Centerline void fraction
ρ_L = Density of liquid
ρ_G = Density of vapor
ϵ = Turbulent viscosity
ν = Kinematic viscosity
μ_L = Liquid viscosity
σ = Surface tension
$\tau_{rr_L} = -\rho_L \overline{v^2}$
$\tau_{\theta\theta_L} = -\rho_L \overline{w^2}$

REFERENCES

BANKOFF, S. G. 1960 A variable density single-fluid model for two-phase flow with particular reference to steam–water flow. *J. Heat Transfer* **82** (2), 265–270.

BEATTIE, D. R. H. 1972 Two-phase flow structure and mixing length theory. *J. nucl. Engng Des.* **21,** 46–64.

DELHAYE, J. M. 1969 General equations of two-phase systems and their applications to air-water bubble flow and to steam–water flashing flow. Presented at *11th Heat Transfer Conf.*, Minneapolis, Minn., ASME Paper 69-HT-63.

DREW, D. 1983 Mathematical modeling of two-phase flow. *A. Rev. Fluid Mech.* **15,** 261–291.

DREW, D. & LAHEY, R. T. 1979 Application of general constitutive principles to the derivation of multidimensional two-phase flow equations. *Int. J. Multiphase Flow* **5,** 243–264.

DREW, D. & LAHEY, R. T. 1981 Phase distribution mechanisms in turbulent two-phase flow in channels of arbitrary cross section. *J. Fluid Engng* **203,** 583–589.

DREW, D. & LAHEY, R. T. 1982 Phase distribution mechanisms in turbulent two-phase flow in a circular pipe. *J. Fluid Mech.* **117,** 91–106.

DREW, D., LAHEY, R. T. & SIM, S. 1978 Radial phase distribution mechanisms in two-phase flows. In *Proc. OECD/CSNI Special. Mtg on Transient Two-phase Flow*, Paris.

EICHHORN, R. & SMALL, S. 1964 Experiments on the lift and drag of spheres suspended in a Poiseuille flow. *J. Fluid Mech.* **20,** 513–527.

INOUE, A., AOKI, S., KOGA, T. & YAEGASHI, H. 1976 Void fraction, bubble and liquid velocity profiles of two-phase flow in a vertical pipe. *Trans. JSME* **42,** 2521–2531.

ISHII, M. 1975 *Thermal–Fluid Dynamics of Two-phase Flow.* Eyrolles, Paris.

KOBAYASHI, K., IIDA, Y. & KANEGAE, N. 1970 Distribution of local void fraction of air–water two-phase flow in a vertical channel. *Bull. JSME* 1005–1012.

LAHEY, R. T. & DREW, D. 1979 The analysis of phase distribution in fully developed two-phase flow. In *Proc. 2nd Multiphase Flow and Heat Transfer Symp.-Wkshp.* Hemisphere, Washington, D.C.

LANCE, M. 1979 Contribution à l'étude de la turbulence dans la phase liquide des écoulements à bulles. Ph.D. Thesis, University Claude Bernard De Lyon, France.

LANCE, M., MARIÉ, J. L., CHARNEY, G. & BATAILLE, J. 1980 Turbulent structure of a co-current air–water bubbly flow. In *Proc. ANS/ASME/NRC Int. Top. Mtg on Nuclear Reactor Thermal-Hydraulics*, Saratoga, N.Y.

LAUFER, J. 1952 Investigation of turbulent flow in a two-dimensional channel. NACA Report 1053.

LAUFER, J. 1953 The structure of turbulence in fully developed pipe flow. NACA Report 1273.

LEVY, S. 1963 Prediction of two-phase pressure drop and density distribution from mixing length theory. *J. Heat Transfer* **85,** (2), 137–152.

MALNES, D. 1966 Slip ratios and fraction factors in the bubble flow region in vertical tubes. Report KR-110, Institutt for Atomenergi, Kjelles, Norway.

MARIE, J. L. & LANCE, M. 1983 Turbulence measurements in two-phase bubbly flows using laser

MARIÉ, J. L. & LANCE, M. 1983 Turbulence measurements in two-phase bubbly flows using laser Doppler anemometry. In *Measuring Techniques in Gas–Liquid Two-phase Flows* (Edited by DELHAYE, J. M. & COGNET, G.), pp. 141–148. Springer, New York.

OSHINOWA, T. & CHARLES, M. E. 1974 Vertical two-phase flow, Pt 1. Flow pattern correlations. *Can. J. chem. Engng* **52,** 25–35.

SERIZAWA, A. 1974 Fluid-dynamic characteristics of two-phase flow. Ph.D. Thesis, Kyoto Univ., Japan.

SERIZAWA, A. & MICHIYOSHI, I. 1984 turbulence in two-phase bubbly flow. In *Proc. of Japan–U.S. Semin. on Two-phase Flow Dynamics*, Lake Placid, N.Y.

SERIZAWA, A., KATAOKA, I. & MICHIYOSHI, I. 1974a Turbulence structure of air–water bubbly flow–I. Measuring techniques. *Int. J. Multiphase Flow* **2,** 221–233.

SERIZAWA, A., KATAOKA, I. & MICHIYOSHI, I. 1974b Turbulence structure of air–water bubbly flow–II. Local properties. *Int. J. Multiphase Flow* **2,** 235–246.

SERIZAWA, A., KATAOKA, I. & MICHIYOSHI, I. 1974c Turbulence structure of air–water bubbly flow—III. Transport properties. *Int. J. Multiphase Flow* **2,** 247–259.

SERIZAWA, A., TSUDA, K. & MICHIYOSHI, I. 1983 Real-time measurement of two-phase flow turbulence using dual-sensor anemometry. Presented at *IUTAM Symp. of Measuring Techniques in Gas–Liquid Two-phase Flows*, Nancy, France. Hemisphere, Washington, D.C.

SULLIVAN, J. P., HOUGE, R. N., BUENGER, D. E. & THEOFANOUS, T. G. 1978 Turbulence in two-phase flows. Presented at *Spec. Mtg. on Transient Two-phase Flow*, OECD/CSNI, Paris.

THEOFANOUS, T. G. & SULLIVAN, J. P. 1982 Turbulence in two-phase dispersed flows. *J. Fluid Mech.* **116,** 343–362.

THOMAS, N. H., AUTON, R. T., SEVE, K. & HUNT, J. C. R. (1983) Entrapment and transport of bubbles by transient large eddies in multiphase turbulent shear flows. Presented at *Int. Conf. on the Physical Modeling of Multiphase Flow*, Coventry, U.K.

TSUJI, Y., MORIKAWA, Y. & SHIOMI, H. 1984 LDV measurements of an air–solid two-phase flow in a vertical pipe. *J. Fluid Mech.* **139,** 417–434.

WALLIS, G. B. 1969 *One-dimensional Two-phase Flow*. McGraw-Hill, New York.

WANG, S. K. 1985 Three-dimensional turbulence structure measurements in air/water two-phase flows. Ph.D. Thesis, Rensselaer Polytechnic Institute, Troy, N.Y.

WANG, S. K., LEE, S. J., JONES, O. C. JR & LAHEY, R. T. JR 1984 Local void fraction measuring techniques in two-phase flow using hot-film anemometry. In *ASME Symposium Volume G-00247.*

ZUBER, N., STARK, F. W., BIJWAARD, G. & KROEGER, P. G. 1967 Steady-state and transient void fraction in two-phase flow systems. Report GEAP-5417.

APPENDIX

Radial Pressure Distribution

If we eliminate M_L by adding [12a] to [12b], we obtain

$$\frac{\partial p}{\partial r} + \frac{1}{r}\frac{\mathrm{d}}{\mathrm{d}r}\left(\alpha r \tau_{rr_G}\right) - \frac{1}{r}\alpha\tau_{\theta\theta_G} + \frac{1}{r}\frac{\mathrm{d}}{\mathrm{d}r}\left[r(1-\alpha)\,\tau_{rr_L}\right] - \frac{1}{r}(1-\alpha)\,\tau_{\theta\theta_L} = 0. \qquad [A.1]$$

If we neglect viscous effects in the vapor (i.e. set $\tau_{rr_G} = \tau_{\theta\theta_G} = 0.0$) and substitute for the turbulent stress terms,

$$\tau_{rr_L} = -\rho_L \overline{v^2}$$

and

$$\tau_{\theta\theta_L} = -\rho_L \overline{w^2},$$

[A.1] becomes

$$-\frac{\partial p}{\partial r}-\frac{1}{r}\frac{\mathrm{d}}{\mathrm{d}r}\left[r(1-\alpha)\,\rho_{\mathrm{L}}\overline{v^2}\right]+\frac{1}{r}(1-\alpha)\,\rho_{\mathrm{L}}\overline{w^2}=0.$$

This equation can be simplified to

$$\frac{\partial p}{\partial r}-\frac{\mathrm{d}}{\mathrm{d}r}\left[(1-\alpha)\,\rho_{\mathrm{L}}\overline{v^2}\right]-\frac{(1-\alpha)\rho_{\mathrm{L}}(\overline{v^2}-\overline{w^2})}{r}=0.$$

Integrating the above equation yields

$$p(r)=p(R)-(1-\alpha)\,\rho_{\mathrm{L}}\overline{v^2}-\int_R^r\frac{(1-\alpha)\,\rho_{\mathrm{L}}(\overline{v^2}-\overline{w^2})}{r'}\,\mathrm{d}r'. \qquad [A.2]$$

We note that in regions where the turbulent fluctuations (i.e. $\overline{v^2}$, $\overline{w^2}$) are large, the local static pressure, $p(r)$, is reduced.